Determination of Stability Constants of Copper(II)–Lactate Complexes in Cu2O Electrodeposition Baths by UV-vis Absorption Spectra Factor Analysis

AUTHOR(S):

Chen, Tianyu; Kitada, Atsushi; Fukami, Kazuhiro; Murase, Kuniaki

CITATION:

Chen, Tianyu ...[et al]. Determination of Stability Constants of Copper(II)–Lactate Complexes in Cu2O Electrodeposition Baths by UV-vis Absorption Spectra Factor Analysis. Journal of The Electrochemical Society 2019, 166(15): D761-D767

ISSUE DATE:

2019-10-21

URL:

http://hdl.handle.net/2433/244821

Determination of Stability Constants of Copper(II)–Lactate Complexes in Cu_2O Electrodeposition Baths by UV-vis Absorption Spectra Factor Analysis

Tianyu Chen, Atsushi Kitada, Kazuhiro Fukami, * and Kuniaki Murase *,z

Department of Materials Science and Engineering, Kyoto University, Sakyo-ku, Kyoto 606-8501, Japan

The stability constants of highly concentrated copper(II)–lactate alkaline aqueous solutions for Cu_2O electrodeposition were determined by factor analysis of UV-vis absorption spectra. The stability constant is $10^{7.05 \pm 0.05}$ for the chemical equilibrium expression $CuL_2 + OH^- = Cu(H_{-1}L)L^- + H_2O$, while that for the chemical equilibrium expression $Cu(H_{-1}L)L^- + OH^- = Cu(H_{-1}L)_2^{2-} + H_2O$ is $10^{5.05 \pm 0.05}$; here, L^- is the lactate ion ($CH_3CH(OH)COO^-$) and $H_{-1}L^{2-}$ is the deprotonated lactate ion ($CH_3CH(O^-)COO^-$). By refining the potential–pH and pH speciation diagrams for the Cu–lactate–H_2O system, it appears that the pH dependence of the preferential orientation of Cu_2O is due to differences in the dissolved species.
 [DOI: 10.1149/2.1231914jes]

Manuscript submitted July 22, 2019; revised manuscript received September 10, 2019. Published October 21, 2019.

Cuprous oxide (Cu_2O) is a low-cost p-type semiconductor with low toxicity that has attracted the attention of researchers as a solar-cell and photocathode material.[1–12] Electrodeposition, commonly from highly concentrated aqueous alkaline solutions of copper(II) salt and lactic acid (HL; $CH_3CH(OH)COOH$), is one of the most popular ways to fabricate Cu_2O thin films.[13]

The dissolved species in aqueous solution have long remained unknown due to issues arising from the direct analysis of concentrated aqueous solutions. In our previous work, we directly analyzed a concentrated solution via probe electrospray ionization mass spectrometry (PESI–MS).[18] The unknown complexes were shown to be $Cu(H_{-1}L)L^-$ and $Cu(H_{-1}L)_2^{2-}$, in which $H_{-1}L^{2-}$ was the lactate ion bearing a deprotonated α-hydroxyl group. However, the stability constants of each complex could not be determined.

Stability constants constitute important thermodynamic data that enable quantitative discussion or the construction of potential–pH and pH speciation diagrams. In this study, a factor analysis of UV-vis absorption spectra was conducted for Cu_2O electrodeposition baths. A set of stability constants of the complexes was presented, and refined potential –pH and pH speciation diagrams were drawn by considering the $Cu(H_{-1}L)L^-$ and $Cu(H_{-1}L)_2^{2-}$ complexes. In copper(II)-lactate alkaline solutions, the preferential crystal orientation of Cu_2O electrodeposits depends on pH, i.e., <100> at pH 8.2–9.5 and <111> at pH 10.5–12.5. K. Mizuno et al. speculated that the change in the dissolved copper complexes causes a change in the preferred orientation of Cu_2O.[14] Other studies also mentioned the influence of bath pH on the preferred orientation.[13–17] However, none of those studies provided a convincing explanation for this phenomenon, since the dissolved copper complex(es) remained undetermined and the pH dependence of the Cu_2O orientation needed further explanation. In this work, the relationship between the dissolved species and the preferential orientation of the Cu_2O deposits is also discussed.

Experimental

Preparation of sample solutions.—For recording the UV-vis absorption spectra, 30 sets of 15-mL aqueous solutions of 0.4 mol dm^{-3} copper(II)–3.0 M lactate[18] were used as the analytes. Each sample contained 0.06 mol (2.25 g) $Cu(ClO_4)_2 \cdot 6H_2O$ (99%, Nacalai Tesque) and 0.045 HL (3.75 mL) (91.1%, Nacalai Tesque). The pH of each sample was adjusted using solid NaOH (97%, Nacalai Tesque). As mentioned in our previous work, Cu(II)–lactate complexation required at least 24 h to reach chemical equilibrium.[18] To ensure completion of the complexation processes, these samples were then stored in 20-mL airtight screw tubes for one week. The pH values were measured at 25°C using a pH meter (HORIBA D–51; Horiba) with a glass electrode (HORIBA 9615–10D; Horiba); the results are summarized in Table I. To avoid alkaline error, the glass electrode was successively washed before each use with 1 M hydrochloric acid and an aqueous solution of 10% thiourea/1% HCl, for 1 h each. In addition, the pH was calibrated using commercially available pH standard solutions.

Measurement of UV-Vis absorption spectra.—The UV-vis absorption spectra were measured with a double-beam spectrometer (Hitachi U-3500). Quartz cells having an optical path length of 1 mm (CELL TYPE 15-S-1, GL Sciences, Inc., Japan) were used, with deionized water as the reference. The spectra were obtained in the range of

Table I. Amount of added NaOH.[18]

Number	NaOH/g	c_{NaOH}/M	pH
1	0.00	0.00	0.34
2	0.20	0.33	0.67
3	0.39	0.65	1.40
4	0.59	0.98	1.94
5	0.78	1.30	2.72
6	1.00	1.67	3.13
7	1.20	2.00	3.52
8	1.40	2.33	4.08
9	1.59	2.65	4.74
10	1.80	3.00	6.04
11	1.83	3.05	6.22
12	1.87	3.10	6.36
13	1.89	3.15	6.62
14	1.91	3.19	6.79
15	1.95	3.25	6.96
16	1.99	3.30	7.02
17	2.01	3.35	7.11
18	2.04	3.40	7.80
19	2.07	3.45	7.95
20	2.10	3.50	7.98
21	2.13	3.55	8.23
22	2.16	3.60	8.38
23	2.19	3.65	8.53
24	2.22	3.70	8.90
25	2.25	3.75	9.18
26	2.28	3.80	9.55
27	2.34	3.90	12.41
28	2.40	4.00	12.79
29	2.46	4.10	13.06
30	2.52	4.20	13.15

*Electrochemical Society Member.
zE-mail: murase.kuniaki.2n@kyoto-u.ac.jp

849–550 nm, which is the main absorption range of Cu(II), at 1-nm intervals. The absorbance data were multiplied by 10 in order to produce data equivalent to those typically generated with an optical path length of 1 cm.

Factor analysis.—According to our previous work, copper(II)–lactate complexes dissolved in the neutral and alkaline region are highly sensitive and can exist only in concentrated aqueous solution; we proved that $Cu(OH)_2$ precipitated after dilution, even when the pH was adjusted to the same value (e.g., pH 9.5). Three species, i.e., CuL_2, $Cu(H_{-1}L)L^-$, and $Cu(H_{-1}L)_2^{2-}$, are in equilibrium in this region, and the absorption spectra strongly overlap.[18] Therefore, a method that can analyze the copper(II)–lactate system while maintaining the original experimental conditions (i.e., concentration and equilibrium relationship) is desired.

The factor analysis method fulfills these requirements. Gampp et al. explained factor analysis for the absorption spectra of chemical species in detail.[19–22] According to Lambert-Beer's law, the absorption of a certain species can be described by the following equation:

$$\boldsymbol{A}_{\lambda k} = \Sigma \boldsymbol{\varepsilon}_{\lambda j} \boldsymbol{c}_{jk} \boldsymbol{l} \qquad [1]$$

where $\boldsymbol{A}_{\lambda k}$ is the total absorbance of the whole compounds in the kth sample, λ nm refers to the wavelength of transmitted light, $\boldsymbol{\varepsilon}_{\lambda j}$ is the absorption coefficient of the jth dissolved compound at λ nm, $\boldsymbol{c}_{jk}$ is the concentration of the jth compound in the kth sample, and $\boldsymbol{l}$ is a constant pertaining to the optical path length (1 cm).

The spectral data can be written in matrix notation: $\mathbf{D} = \mathbf{RC}$. $\mathbf{D}$ is the data matrix consisting of the measured absorbance data, which has λ rows (wavelength) and k columns (number of samples). The aim of factor analysis is to determine the exact spectral matrix $\mathbf{R}$ and composition matrix $\mathbf{C}$ from the data matrix $\mathbf{D}$. There are limited possibilities for a wide range $\mathbf{R}$ and $\mathbf{C}$ that fulfill the equation $\mathbf{D} = \mathbf{RC}$ mathematically, while generating physically and chemically meaningful matrixes. In this work, we determined a set of physically and chemically meaningful $\mathbf{R}$ and $\mathbf{C}$ by assuming chemical equilibria between the optical active species,[24,25] i.e., the copper(II)–lactate complexes, using the equilibrium constants as fitting parameters. The factor analysis in this work involved two steps.[22] The first step was principal component analysis (PCA), by which the number of optical active species as well as their chemical equilibria could be determined. The PCA calculations here were performed using Maple 2018 software (Waterloo Maple Inc.). The second step was evolution factor analysis (EFA), where the optimum $\mathbf{R}$ and $\mathbf{C}$ were determined by the simplex method.[23] A homemade calculation program developed in C++, which refers to work by Ozeki et al.,[24,25] was used to perform the EFA step.

Results and Discussion

Measurement of absorption spectra.—The UV-vis absorption spectra of thirty 0.4 M Cu(II) and 3.0 M HL aqueous solution samples, ranging in pH from 0.34 to 13.15, are shown in Figure 1. In the pH range 0.34–4.74, the absorbance increased with increasing pH. A slight blueshift of the copper(II) *d-d* transition was observed, indicating that the dissolved copper(II) species had changed, while no isosbestic points were observed in this region. For the absorption spectra at pH 6.04–7.11, an isosbestic point was observed at approximately 750 nm, while an additional isosbestic point was observed at approximately 600 nm for those at pH 7.80–13.15. The observation of isosbestic points indicated that only two optically active copper(II)–containing species were in equilibrium. In our previous work,[18] we concluded that five copper(II)–lactate complexes, i.e., Cu^{2+}, CuL^+, CuL_2, $Cu(H_{-1}L)L^-$, and $Cu(H_{-1}L)_2^{2-}$, exist in the 0.4 M copper(II)–3.0 M lactate aqueous solution. The chemical equilibrium in each pH range can be given as follows:

$$Cu^{2+} + L^- = CuL^+ \qquad (0.34 < pH < 4.74) \qquad [2.1]$$

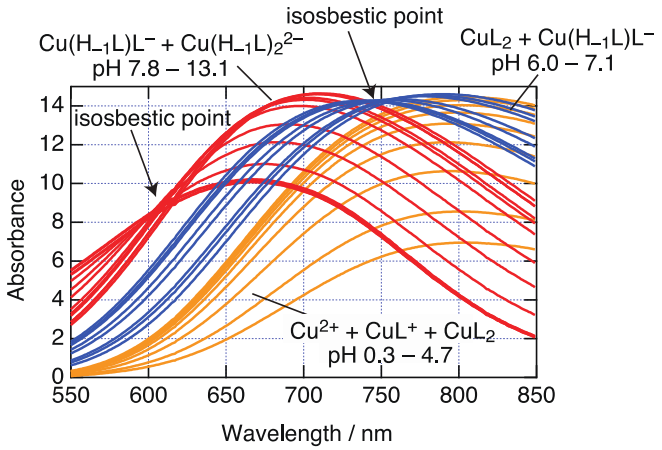

Figure 1. The absorption spectra of 0.4 M Cu(II)–3.0 M HL aqueous solution with pH values ranging from 0.34 to 13.15.

and/or

$$Cu^{2+} + HL = CuL^+ + H^+ \qquad [2.2]$$

$$CuL^+ + L^- = CuL_2 \qquad [3.1]$$

and/or

$$CuL^+ + HL = CuL_2 + H^+ \qquad [3.2]$$

$$CuL_2 + OH^- = Cu(H_{-1}L)L^- + H_2O \qquad (6.04 < pH < 7.11) \qquad [4]$$

$$Cu(H_{-1}L)L^- + OH^- = Cu(H_{-1}L)_2^{2-} + H_2O \qquad (7.80 < pH < 13.15) \qquad [5]$$

Factor analysis of Cu(II)–lactate baths.—In the factor analysis, we first performed PCA to confirm that the copper(II)–lactate system could be analyzed. The measurement spectral data for matrix $\mathbf{D}$ constitute a 300 × 30 matrix. The 300 rows refer to the scanning wavelengths from 849 nm to 550 nm at 1-nm intervals, while the 30 columns denote the number of samples. The 30 × 30 covariance matrix $\mathbf{Z}$ of matrix $\mathbf{D}$ is given by $\mathbf{Z} = {}^t\mathbf{DD}$. The eigenvalues of matrix $\mathbf{Z}$ were calculated, and the results are summarized in Table II. The magnitude of the eigenvalues indicates the significance of the chemical species. For the entire pH region (0.34–13.15), there are five significant eigenvalues out of the thirty values; 833543.6509, 45490.9177, 425.2038, 10.0912, and 4.0186. These five significant eigenvalues refer to the five copper(II) species in the copper(II)–lactate solution mentioned above. The eigenvalues of each region also agree with our previous conclusion. In the pH range of 0.34–4.74, there are three significant eigenvalues (204637.3438, 100.7759, and 6.1888), indicating that three copper(II) lactate complexes (Cu^{2+}, CuL^+, and CuL_2) exist. In the pH range of 6.04–13.15, there are three significant eigenvalues, 648698.1852, 25774.8143, and 255.1911, which are the principal factors. These results confirmed that only three optical active species, CuL_2, $Cu(H_{-1}L)L^-$, and $Cu(H_{-1}L)_2^{2-}$, existed in these solutions. Moreover, only two significant eigenvalues, 291864.4077 and 1555.0453, were obtained from the solutions for pH 6.04–7.11, confirming that only two copper(II)–containing species, CuL_2 and $Cu(H_{-1}L)L^-$, were in equilibrium in this region. Although 3.9724 should be considered as a principal factor due to the small quantity of existing CuL_2, only two significant eigenvalues, 374403.0872 and 6902.8214, were obtained from the solutions for pH 7.80–13.15. This confirmed that mainly two copper(II)–lactate complexes, $Cu(H_{-1}L)L^-$ and $Cu(H_{-1}L)_2^{2-}$, were in equilibrium in this region. Thus, the PCA results matched with our previous conclusion from the experimental data. The PCA confirmed that the dissolved copper(II)–lactate complexes in 0.4 M Cu(II)–3.0 M HL

Table II. Eigenvalues of matrix Z. Numbers in bold type indicate significant eigenvalues.

		Eigenvalues				
#	pH	0.34–13.15	0.34–4.74	6.04–13.15	6.04–7.11	7.80–13.15
1		**833543.6509**	**204637.3438**	**648698.1852**	**291864.4077**	**374403.0872**
2		**45490.9177**	**100.7759**	**25774.8143**	**1555.0453**	**6902.8214**
3		**425.2038**	**6.1888**	**255.1911**	0.1193	**3.9724**
4		**10.0912**	0.0233	1.3123	0.0015	0.1449
5		**4.0186**	0.0039	0.1310	0.0011	0.0724
6		0.0867	0.0009	0.0336	0.0006	0.0044
7		0.0266	0.0010	0.0064	0.0007	0.0017
8		0.0098	0.0011	0.0020	0.0009	0.0009
9		0.0033	0.0011	0.0015	/	0.0008
10		0.0017	/	0.0010	/	0.0005
11		0.0013	/	0.0009	/	0.0005
12		0.0012	/	0.0008	/	0.0006
13		0.0011	/	0.0008	/	0.0007
14		0.0004	/	0.0008	/	/
15		0.0010	/	0.0004	/	/
16		0.0010	/	0.0007	/	/
17		0.0010	/	0.0006	/	/
18		0.0004	/	0.0007	/	/
19		0.0009	/	0.0005	/	/
20		0.0005	/	0.0006	/	/
21		0.0005	/	0.0005	/	/
22		0.0005	/	/	/	/
23		0.0006	/	/	/	/
24		0.0006	/	/	/	/
25		0.0007	/	/	/	/
26		0.0007	/	/	/	/
27		0.0007	/	/	/	/
28		0.0008	/	/	/	/
29		0.0008	/	/	/	/
30		0.0008	/	/	/	/

aqueous solution could be explained by five eigenvectors for the whole pH range and three eigenvectors for the alkaline region of concern. After the PCA step, an initial set of spectral matrix $\mathbf{R_0}$ and composition matrix $\mathbf{C_0}$ was obtained. However, these matrixes were physicochemically meaningless and could be optimized by considering the chemical equilibrium in the EFA step.

The flow chart of EFA is shown in Figure 2. In this step, the chemical equilibria of the dissolved copper(II)-containing species with the stability constants (Table III) were considered to specify the exact **R** and **C**. In Table III, K_i refers to the initial unoptimized stability constants of each chemical equilibrium. The stability constants K_{1i}–K_{3i} were obtained from Ref. 26, and the equilibrium constants K_{4i} and K_{5i} were obtained from the following equations:

$$\log K_{4i} \approx -\log\left[OH^-\right] - \log\left[CuL_2\right] / \left[Cu\left(H_{-1}L\right)L^-\right] \quad [6]$$

$$\log K_{5i} \approx -\log\left[OH^-\right] - \log\left[Cu\left(H_{-1}L\right)L^-\right] / \left[Cu(H_{-1}L)_2{}^{2-}\right] \quad [7]$$

where $[CuL_2] = [Cu(H_{-1}L)L^-]$ and $[Cu(H_{-1}L)L^-] = [Cu(H_{-1}L)_2{}^{2-}]$, while K_{4i} and K_{5i} are equal to –log[OH^-] (pOH). Figure 3 shows the fraction diagrams used to determine the initial complexation constants, from which K_{4i} and K_{5i} were determined to be $10^{7.25}$ and $10^{4.85}$, respectively.

In this work, we failed to obtain convincing K_2 and K_3 values, since the *d-d* transition absorption bands of Cu^{2+}, CuL^+, and CuL_2 overlapped strongly without an isosbestic point. Thus, the spectrum cannot be divided accurately, resulting in a random EFA result for region I. However, since the ionic strength I of the samples in region I (pH 0.34–4.74) in this work ranged from 0.85 to 2.75, it is reasonable to accept the reported stability constants in Ref. 26 as optimized values, which were obtained at $I = 1.0$–2.0. In contrast, reliable results of K_4 ($10^{7.05 \pm 0.05}$) of $Cu(H_{-1}L)L^-$ and K_5 ($10^{5.05 \pm 0.05}$) of $Cu(H_{-1}L)_2{}^{2-}$ were obtained.

The optimized stability constants K_4 and K_5 are given in Table III. The spectral matrixes of CuL_2, $Cu(H_{-1}L)L^-$, and $Cu(H_{-1}L)_2{}^{2-}$ were also obtained, based on which the absorption spectra of each pure complex are illustrated in Figure 4. The simulation of the absorption spectra, which was based on the spectral matrixes and stability constants obtained in this work, is shown in Figure 5. It can be inferred from Figure 5 that the simulated absorption spectra of region II and region III fit well with the experimental data. Figure 6 shows a

Table III. Stability constants of copper(II)–lactate complexes.

	Reaction	Log K_i	Fitted Log K	Ref.
(1)	$HL = H^+ + L^-$	–3.81	–3.81 ± 0.01	26
(2)	$Cu^{2+} + L^- = CuL^+$	2.45	2.45 ± 0.05	26
(3)	$Cu^{2+} + 2L^- = CuL_2$	4.08	4.08 ± 0.1	26
(4)	$CuL_2 + OH^- = Cu(H_{-1}L)L^- + H_2O$	7.25	7.05 ± 0.05	This work
(5)	$Cu(H_{-1}L)L^- + OH^- = Cu(H_{-1}L)_2{}^{2-} + H_2O$	4.75	5.05 ± 0.05	This work

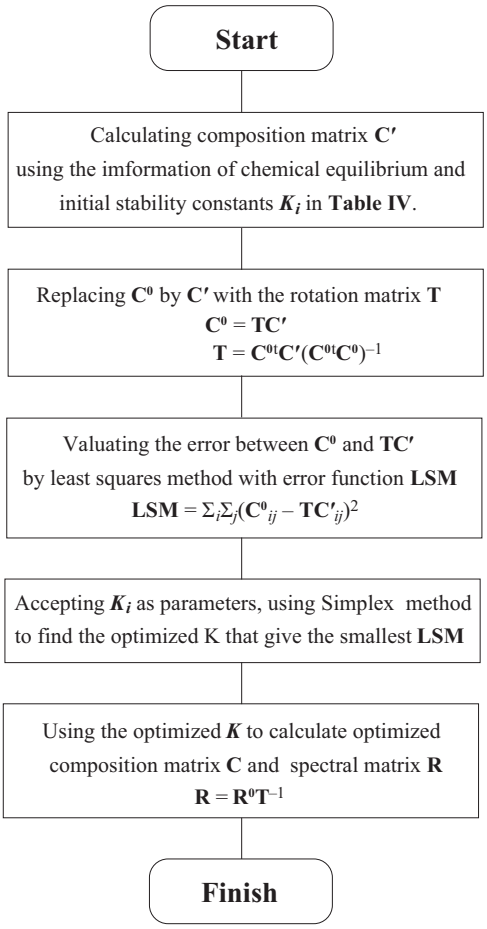

Figure 2. The flow chart of EFA step in this work.

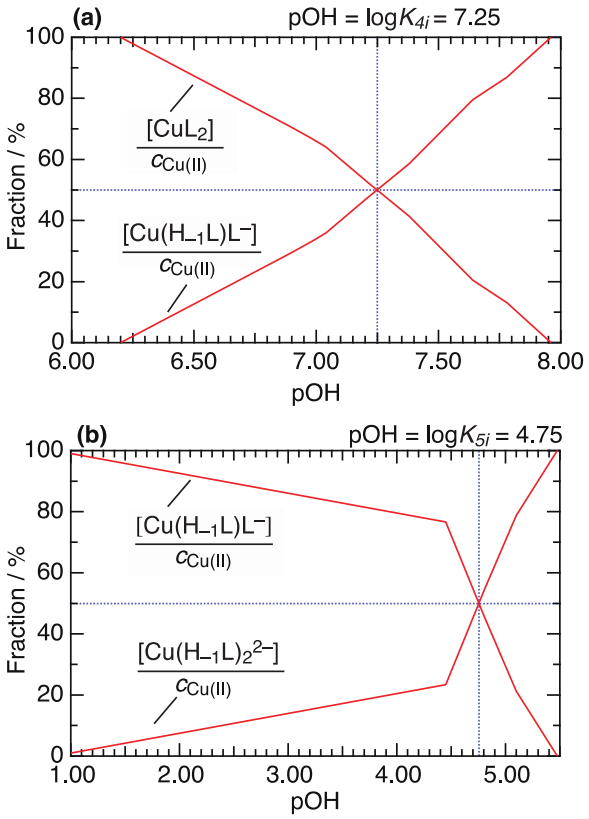

Figure 3. The fraction diagrams used to determine the initial complexes constants of $Cu(H_{-1}L)L^-$ and $Cu(H_{-1}L)_2^{2-}$.

comparison between the simulated titration plot, which was calculated from the information in Table IV, and the experimental data. The simulated titration plot fitted well with the experimental data in the low-pH region (region I), indicating the applicability of the stability constants in Ref. 26. Moreover, the simulated plot in the mid–high pH region matched well with the experimental data. Therefore, both the simulation of the absorption spectra and the titration plot proved that the EFA results of this work are reliable.

Refined potential–pH diagram and pH speciation diagram.—According to the potential–pH diagram of the Cu–H_2O system (Fig. 7a), the stability region of Cu_2O(s) lies mainly in the neutral–alkaline region, where no stable dissolved Cu(II)-containing species exist. Therefore, to prepare an electrodeposition bath for Cu_2O deposition, it is necessary to add a ligand that can complex with the copper(II) ion to form the desired stable dissolved complex in the alkaline region. The lactate ion L^- is a suitable ligand, and an alkaline aqueous 0.4 M copper(II)–3.0 M lactate solution of pH 9.0–12.5 has been successfully used as the electrodeposited bath to fabricate Cu_2O film.[13–16] However, the potential–pH diagram of the Cu–HL–H_2O system based on reported thermochemical data (Fig. 7b) indicates that $Cu(OH)_2$

Table IV. Thermochemical data used for the potential–pH diagram calculation.

I. Species and Chemical potentials

Species	State	μ^o (298 K, kJ mol^{-1})	Ref.
Cu	Crystal	0	27
Cu^{2+}	Aqueous	64.98	27
Cu_2O	Crystal	–146.36	27
H_2O	Aqueous	–237.19	27
H^+	Aqueous	0	27
O_2	Gas	0	27
H_2	Gas	0	27

II. Reactions and Stability Constants

Reaction	log$K$	Ref.
$HL = H^+ + L^-$	–3.81	26
$Cu^{2+} + L^- = CuL^+$	2.45	26
$Cu^{2+} + 2L^- = CuL_2$	4.08	26
$Cu^{2+} + 2L^- = Cu(H_{-1}L)L^- + H^+$	–2.87	This work
$Cu^{2+} + 2L^- = Cu(H_{-1}L)_2^{2-} + 2H^+$	–11.82	This work

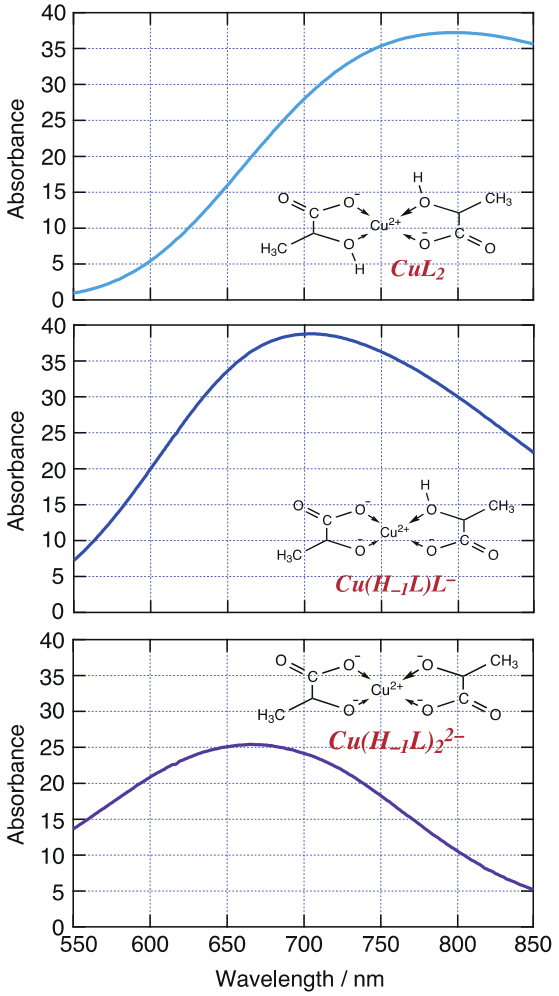

Figure 4. The absorption spectra of pure CuL_2, $Cu(H_{-1}L)L^-$ and $Cu(H_{-1}L)_2^{2-}$ obtained by EFA in this work.

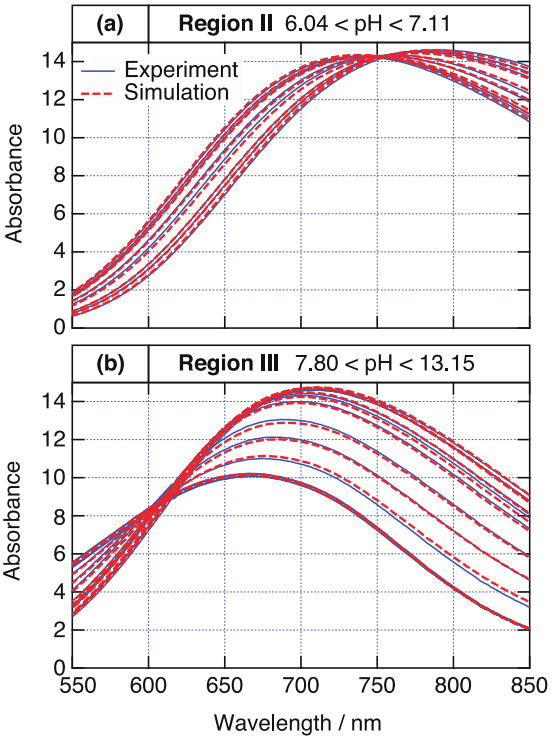

Figure 5. (a) Comparison of simulated absorption spectra, using the EFA results from this work, and experimental data in region II; and (b) the same comparison in region III.

precipitates at pH > 8.0, which is inconsistent with the experimental results. In contrast, we also confirmed the formation of the $Cu(OH)_2$ precipitate during the dilution of 0.4 M copper(II)–3.0 M lactate solution with deionized water above pH 8.0,[18] which corresponded with the data shown in Figure 7b. These results indicated that the reported thermochemical data were insufficient to discuss the concentrated copper(II)-lactate system in the alkaline region.

The refined potential–pH diagram of the copper–lactate system and the refined pH–speciation diagram of the copper(II)–lactate system are shown in Figures 7c and 8, respectively; the thermochemical data and equilibrium reactions used to calculate these graphs are displayed in Tables IV and V. Note that the activities of the dissolved species correlate to concentration. As shown in Figures 7c and 8, two dissolved complexes, $Cu(H_{-1}L)L^-$ and $Cu(H_{-1}L)_2^{2-}$, exist in the alkaline region of the 0.4 M copper(II)–3.0 M lactate aqueous solution, instead of the $Cu(OH)_2$ precipitate.

Discussion of the relationship between dissolved complexes and preferential orientation of Cu_2O.—For Cu_2O–ZnO solar cells, <111>-oriented Cu_2O is favored because the (111)-Cu_2O/(0001)-

Table V. List of equilibrium reactions and conditions considered to calculate the potential–pH diagrams of Cu–HL–H_2O system and H_2O–O_2 system.

I. The Cu–HL–H_2O system		
1	$Cu^{2+} + HL = CuL^+ + H^+$	$pH = 1.36 + \log([CuL^+]/[Cu^{2+}]) - \log[HL]$
2	$CuL^+ + HL = CuL_2 + H^+$	$pH = 2.18 + \log([CuL_2]/[CuL^+]) - \log[HL]$
3	$CuL_2 = Cu(H_{-1}L)L^- + H^+$	$pH = 6.95 + \log([Cu(H_{-1}L)L^-]/[CuL_2])$
4	$Cu(H_{-1}L)L^- = Cu(H_{-1}L)_2^{2-} + H^+$	$pH = 8.95 + \log([Cu(H_{-1}L)_2^{2-}]/[Cu(H_{-1}L)L^-])$
5	$Cu^{2+} + 2e = Cu$	$E(V) = 0.337 + 0.0295[Cu^{2+}]$
6	$CuL^+ + H^+ + 2e = Cu + HL$	$E(V) = 0.377 + 0.0295(\log[CuL^+] - \log[HL] - pH)$
7	$CuL_2 + 2H^+ + 2e = Cu + 2HL$	$E(V) = 0.441 + 0.0295(\log[CuL_2] - 2\log[HL] - 2pH)$
8	$CuL_2 + 2e = Cu + 2L^-$	$E(V) = 0.216 + 0.0295(\log[CuL_2] - 2\log[L^-])$
9	$2CuL_2 + H_2O + 2e = Cu_2O + 2H^+ + 4L^-$	$E(V) = -0.039 + 0.0591(\log[CuL_2] - 2\log[L^-] + pH)$
10	$2Cu(H_{-1}L)L^- + H_2O + 2e = Cu_2O + 4L^-$	$E(V) = 0.371 + 0.0591(\log[Cu(H_{-1}L)L^-] - 2\log[L^-])$
11	$2Cu(H_{-1}L)_2^{2-} + H_2O + 2H^+ + 2e = Cu_2O + 4L^-$	$E(V) = 0.903 + 0.0591(\log[Cu(H_{-1}L)_2^{2-}] - 2\log[L^-] - pH)$
12	$Cu_2O + 2H^+ + 2e = 2Cu + H_2O$	$E(V) = 0.471 - 0.0591pH$
II. The H_2O–O_2 system		
a	$2H^+ + 2e = H_2$	$E(V) = -0.0591pH$
b	$O_2 + 4H^+ + 4e = 2H_2O$	$E(V) = 1.229 - 0.0591pH$

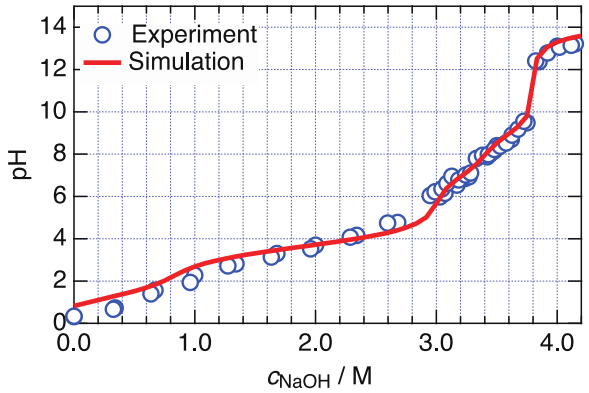

Figure 6. Comparison of simulated pH titration plot, using the complexes constants determined in this work, and experimental data. The analyte is 0.4 M Cu(II) – 3.0 M HL aqueous solution, while the titrant is solid NaOH.

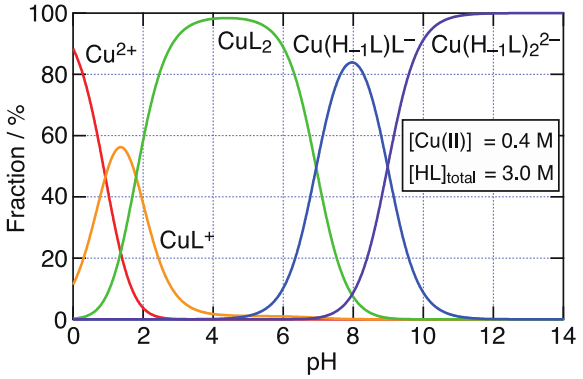

Figure 8. Refined pH speciation diagram of 0.4 M Cu(II)–3.0 M HL aqueous solution.

ZnO heterostructure shows a small lattice mismatch near the interface.[28] It is widely accepted that in copper(II)-lactate solution, the preferential orientation of Cu_2O depends on pH. In most cases, <100> preferential orientation occurs at pH 9.0 and <111> orientation occurs at pH 12.0.[14–16] Wang et al. summarized the pH dependence, confirming that the preferential orientation of deposited Cu_2O was <100> for pH 8.2–9.1, <110> for pH 9.4–9.9, and <111> for pH > 10.2.[17]

The dependence of pH on the preferential orientation of Cu_2O has been discussed by two groups in regard to the crystal growth rate. Shinagawa et al. explained this preferential orientation change of Cu_2O by considering the elementary formation rate of CuOH ($k[Cu^+][OH^-]$), although they did not consider the composition of the dissolved Cu(II) species in detail. The formation of CuOH is the elementary process in the formation of Cu_2O. A larger $[OH^-]$ gives a higher $k[Cu^+][OH^-]$, which results in kinetically-controlled Cu_2O electrodeposition, so that <111> orientation occurs in preference to the thermodynamically favorable <100> orientation.[16] Wang et al. compared the number of oxygen atoms per unit area (N_O) of the crystal planes of Cu_2O, which is 2.78/nm^2 for (100), 5.89/nm^2 for (110), and 8.83/nm^2 for (111). The surface morphology was determined by the crystal surface with the lowest growth rate. Samples deposited at pH < 9.5 (relatively low $[OH^-]$) had the lowest growth rate of {111} because of N_O was the largest in this case, and (100) with the highest growth rate became the preferential orientation. When the pH increased, $[OH^-]$ also increased and the growth of (110) and (111) with a higher N_O was favored, leading to preferential <110> and <111> orientations.[17]

We consider here that the preferential orientation of Cu_2O is affected by not only the growth rate but also the difference in the dissolved complexes. The boundary between the stability region of $Cu(H_{-1}L)L^-$ and $Cu(H_{-1}L)_2^{2-}$ in Figure 7c was pH 9.0, while the preferential orientation of Cu_2O changed from <100> to <110> above pH 9.1.[17] A comparison of the speciation diagram in this work and the pH dependence of deposited Cu_2O orientation, summarized by Wang et al.,[17] is shown in Figure 9. For 8.2 < pH < 9.1, the <100> preferential orientation is reported, and the major dissolved complex is $Cu(H_{-1}L)L^-$ (81.7% to 43.0%). For 9.4 < pH < 9.9, the <110> preferential orientation is also reported, and both $Cu(H_{-1}L)L^-$ (27.5% to 10.7%) and $Cu(H_{-1}L)_2^{2-}$ (72.5% to 89.3%) exist in solution. For pH > 10.2, the <111> preferential orientation is reported, and $Cu(H_{-1}L)_2^{2-}$ (94.7% to 100.0%) is dissolved in solution almost exclusively. Consequently, our results suggest that the quantitative difference in the dissolved complexes caused the orientation change of Cu_2O.

One possible explanation for the effect of the dissolved species on the preferential orientation of deposited Cu_2O is the increase in

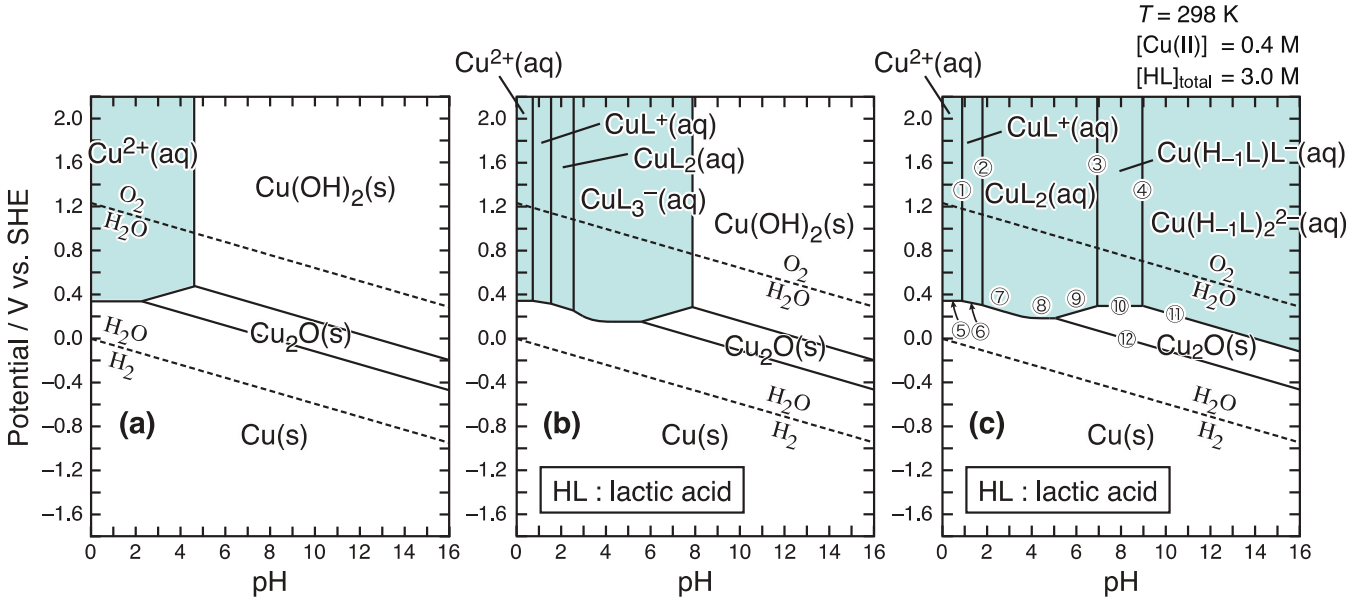

Figure 7. Potential–pH diagram (298 K) of (a) Cu–H_2O system, based on Ref. 27; (b) Cu–HL–H_2O system, based on Ref. 26 and Ref. 27; and (c) refined Cu–HL–H_2O system, based on Ref. 26, Ref. 27 and the results of this work. Note that the analytical concentration of Cu(II) is 0.4 M, and 3.0 M for lactic acid.

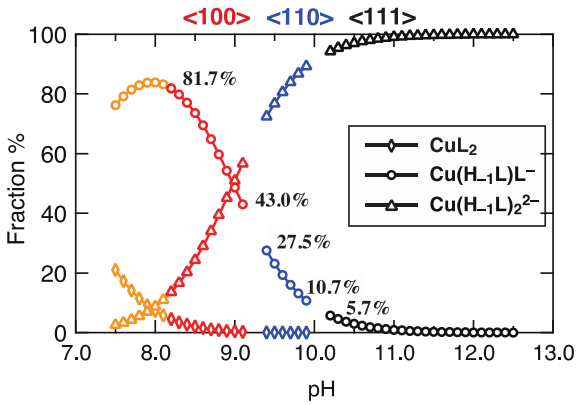

Figure 9. Comparison of the speciation diagram in this work and the pH dependence of deposited Cu_2O orientation summarized by Wang et al.[17] The percentage indicates the ratio of $Cu(H_{-1}L)L^-$.

interfacial pH during the electrodeposition, which may be consistent with the findings of Shinagawa and Wang. During Cu_2O electrodeposition, the half-cell reactions are as follows:

$$2Cu\,(H_{-1}L)\,L^- + H_2O + 2e = Cu_2O + OH^- + 4L^- \quad [8]$$

$$2Cu(H_{-1}L)_2^{2-} + 2H_2O + 2e = Cu_2O + 2OH^- + 4L^- \quad [9]$$

Since OH^- is produced in the reactions, the pH in the vicinity of the working electrode increases. According to the reaction formulas, $Cu(H_{-1}L)L^-$ produces Cu_2O and OH in a 1:1 molar ratio, and $Cu(H_{-1}L)_2^{2-}$ produces Cu_2O and OH in a 1:2 molar ratio. Therefore, the local pH near the electrode/electrolyte interface will be higher when $Cu(H_{-1}L)_2^{2-}$ reacts than when $Cu(H_{-1}L)L^-$ reacts, which favors the <111> orientation according to the aforementioned findings. Following this suggestion, electrodeposition under high overpotential and large current density conditions from $Cu(H_{-1}L)L^-$-dominated solutions also possibly results in Cu_2O with <111> preferential orientation, since acceleration of the chemical reaction will result in more $[OH^-]$ (pH) increase in the vicinity of the working electrode. Another possibility is the $Cu(H_{-1}L)L^-$ and/or $Cu(H_{-1}L)_2^{2-}$ adsorption onto a certain crystallographic plane, which change the surface energy and contribute to a change in the final morphology. To clarify the effect of differences in the concentrations of lactate complexes $Cu(H_{-1}L)L^-$ and $Cu(H_{-1}L)_2^{2-}$ on the orientation of electrodeposited Cu_2O is a future research task. Methods such as in situ surface enhanced Raman spectroscopy and in situ electro-reflectance spectroscopy may help to resolve this issue through study of the adsorption behavior of $Cu(H_{-1}L)L^-$ and $Cu(H_{-1}L)_2^{2-}$ on the working electrode surface during Cu_2O electrodeposition.

Conclusions

We determined the stability constants of copper(II)–lactate complexes in concentrated aqueous solution via factor analysis of the UV-vis absorption spectra. The results were confirmed by comparing the simulated visible absorption spectra and titration curves. A refined pH speciation diagram and a potential–pH diagram of the copper–lactate–water system were drawn using the stability constants from this work. The effect of dissolved copper(II)–lactate complexes on the Cu_2O orientation is also discussed, which gives new insight into the electrodeposition behavior of Cu_2O.

Acknowledgments

This work was supported financially by The Kyoto University Foundation (K. M.) and a Grant-in-Aid for Scientific Research (B) (No. 19H02490: A. K.) from the Japan Society for the Promotion of Science (JSPS).

ORCID

Tianyu Chen https://orcid.org/0000-0003-4663-436X
Atsushi Kitada https://orcid.org/0000-0002-4387-8687
Kazuhiro Fukami https://orcid.org/0000-0001-9120-5578
Kuniaki Murase https://orcid.org/0000-0002-7564-9416

References

1. M. Izaki, T. Shinagawa, K. Mizuno, Y. Ida, M. Inaba, and A. Tasaka, *J. Phys. D. Appl. Phys.*, **40**(11), 3326 (2007).
2. S. S. Jeong, A. Mittiga, E. Salza, A. Masci, and S. Passerini, *Electrochim. Acta*, **53**(5), 2226 (2008).
3. J. Cui and U. J. Gibson, *J. Phys. Chem. C*, **114**(14), 6408 (2010).
4. K. Han and M. Tao, *Sol. Energy Mater. Sol. Cells*, **93**(1), 153 (2009).
5. V. Georgieva and M. Ristov, *Sol. Energy Mater. Sol. Cells*, **73**, 67 (2002).
6. P. E. de Jongh, D. Vanmaekelbergh, and J. J. Kelly, *Chem. Mater.*, **11**(12), 3512 (1999).
7. A. Paracchino, V. Laporte, K. Sivula, M. Gratzel, and Elijah Thimsen, *Nat. Mater.*, **10**, 456 (2011).
8. A. A. Dubale, W. N. Su, A. G. Tamirat, C. J. Pan, B. A. Aragaw, H. M. Chen, C. H. Chen, and B. J. Hwang, *J. Mater. Chem. A*, **2**(43), 18383 (2014).
9. Y. Yang, D. Xu, Q. Wu, and P. Diao, *Sci. Rep.*, **6**, 35158 (2016).
10. P. E. de Jongh, D. Vanmaekelbergh, and J. J. Kelly, *Chem. Commun.*, 1069 (1999).
11. J. N. Nian, C. C. Hu, and H. Teng, *Int. J. Hydrogen Energy*, **33**(12), 2897 (2008).
12. C. C. Hu, J. N. Nian, and H. Teng, *Int. J. Hydrogen Energy*, **92**(9), 1071 (2008).
13. A. E. Rakhshani, A. A. Al-Jassar, and J. Varghese, *Thin Solid Films*, **148**, 191 (1987).
14. K. Mizuno, M. Izaki, K. Murase, T. Shinagawa, M. Chigane, M. Inaba, A. Tasaka, and Y. Awakura, *J. Electrochem. Soc.*, **152**, C179 (2005).
15. T. D. Golden, M. G. Shumsky, Y. Zhou, R. A. VanderWerf, R. A. Van Leeuwen, and J. A. Switzer, *Chem. Mater.*, **8**, 2499 (1996).
16. T. Shinagawa, Y. Ida, K. Mizuno, S. Watase, M. Watanabe, M. Inaba, A. Tasaka, and M. Izaki, *Cryst. Growth Des.*, **13**, 52 (2013).
17. L. C. Wang, N. R. de Tacconi, C. R. Chenthamarakshan, K. Rajeshwar, and M. Tao, *Thin Solid Films*, **515**(5), 3090 (2007).
18. T. Chen, A. Kitada, Y. Seki, K. Fukami, D. T. Usmanov, L. C. Chen, K. Hiraoka, and K. Murase, *J. Electrochem. Soc.*, **165**(10), D444 (2018).
19. H. Gampp, M. Maeder, C. J. Meyer, and A. D. Zuberbuhler, *Talanta*, **32**(2), 95 (1985).
20. H. Gampp, M. Maeder, C. J. Meyer, and A. D. Zuberbuhler, *Talanta*, **32**(4), 257 (1985).
21. H. Gampp, M. Maeder, C. J. Meyer, and A. D. Zuberbuhler, *Talanta*, **32**(12), 1133 (1985).
22. H. Gampp, M. Maeder, C. J. Meyer, and A. D. Zuberbuhler, *Talanta*, **33**(12), 943 (1986).
23. J. A. Nelder and R. Mead, *Comput. J.*, **7**(4), 308 (1965).
24. T. Ozeki, H. Kihara, and S. Hikime, *Bunseki Kagaku*, **35**, 885 (1986).
25. T. Ozeki, H. Kihara, and S. Ikeda, *Anal. Chem.*, **60**, 2055 (1988).
26. E. Martell and R. M. Smith, *Critical Stability Constants, Vol. 5, First Supplement*, p. 291, Plenum Press, New York (1982).
27. M. Pourbaix, *Atlas of Electrochemical Equilibria in Aqueous Solutions*, p. 391, NACE International Cebelcor, Houston (1974).
28. S. Ishizuka, T. Maruyama, and K. Akimoto, *Jpn. J. Appl. Phys.*, **39**(8A), L786 (2000).